Inorganic Chemistry
Communication

Inorg. Chem. **2010**, *49*, 9107–9109 **9107**
DOI: 10.1021/ic1009169

Three-Dimensional Metal−Organic Frameworks Based on Tetrahedral and Square-Planar Building Blocks: Hydrogen Sorption and Dye Uptake Studies

Demin Liu, Zhigang Xie, Liqing Ma, and Wenbin Lin*

Department of Chemistry, CB#3290, University of North Carolina at Chapel Hill, Chapel Hill, North Carolina 27599

Received May 7, 2010

Two three-dimensional metal−organic frameworks (MOFs) with tetraphenylmethane-derived tetracarboxylate linkers and copper paddle-wheel secondary building units were synthesized and characterized by single-crystal X-ray crystallographic studies. The two MOFs show a similar 4,4-connectivity but very different homocrossing and interpenetrating PtS network topologies and exhibit permanent porosity as probed by gas adsorption and dye inclusion experiments.

Metal−organic frameworks (MOFs) have emerged as an interesting new class of hybrid materials that hold great promise in many applications, including gas storage,[1−8] nonlinear optics,[9] chemical sensing,[10−12] catalysis,[13−16] and drug delivery.[17−20] MOFs provide an unprecedented level of synthetic tunability, which allows for the incorporation of limitless building blocks to generate novel functional materials. We have, for example, designed novel heterogeneous asymmetric catalysts by the direct incorporation of catalytic sites into MOFs[15] or by postsynthesis modifications of BINOL-derived chiral porous MOFs.[14] More recently, we have synthesized nanoscale MOFs for delivering anticancer drugs[20] and iridium-containing MOFs for oxygen sensing.[21]

Scheme 1

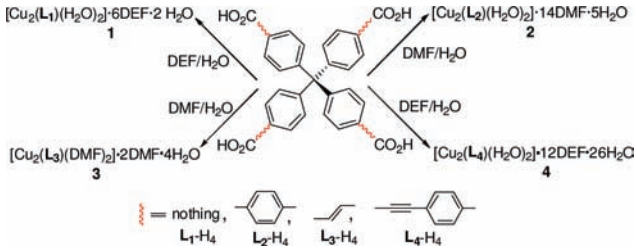

In order to take advantage of the robust 4,4-connected network topology, we have recently constructed MOFs based on bridging ligands of tetrahedral geometry and copper paddle-wheel secondary building units (SBUs).[4,8] We demonstrated that 4,4-connected MOFs **1** and **2** (Scheme 1) could be built from tetraphenylmethane-derived tetracarboxylate ligands $\mathbf{L_1}$ and $\mathbf{L_2}$ and exhibited significant hydrogen uptake and interesting breathing effects upon removal of the included solvents by freeze-drying.[22] In this paper, we report the synthesis of two new tetracarboxylic acids, $\mathbf{L_3}$-H_4 and $\mathbf{L_4}$-H_4, based on the tetraphenylmethane moiety (Scheme 1) and the construction of new 4,4-connected MOFs **3** and **4** (Scheme 1). The permanent porosity of these new MOFs was established by gas uptake and dye inclusion studies.

$\mathbf{L_3}$-H_4 was synthesized by a palladium-catalyzed Heck coupling between tetrakis(4-bromophenyl)methane (**a**)[23,24] and methyl acrylate followed by base-catalyzed hydrolysis

*To whom correspondence should be addressed. E-mail: wlin@unc.edu.

(1) Rosi, N. L.; Eckert, J.; Eddaoudi, M.; Vodak, D. T.; Kim, J.; O'Keeffe, M.; Yaghi, O. M. *Science* **2003**, *300*, 1127.
(2) Dincă, M.; Yu, A. F.; Long, J. R. *J. Am. Chem. Soc.* **2006**, *128*, 8904.
(3) Kesanli, B.; Cui, Y.; Smith, R. M.; Bittner, W. E.; Bockrath, C. B.; Lin, W. *Angew. Chem., Int. Ed.* **2005**, *44*, 72.
(4) Ma, L.; Lin, W. *Angew. Chem., Int. Ed.* **2009**, *48*, 3637.
(5) Lin, X.; Jia, J.; Zhao, X.; Thomas, K. M.; Blake, J. A.; Gavin, W. S.; Champness, R. N.; Hubberstey, P.; Schröer, M. *Angew. Chem., Int. Ed.* **2006**, *45*, 7358.
(6) Ma, L.; Mihalcik, D. J.; Lin, W. *J. Am. Chem. Soc.* **2009**, *131*, 4610.
(7) Ma, S.; Sun, D.; Ambrogio, M.; Fillinger, J. A.; Parkin, S.; Zhou, H. *J. Am. Chem. Soc.* **2007**, *129*, 1858.
(8) Ma, L.; Lee, J. Y.; Li, J.; Lin, W. *Inorg. Chem.* **2008**, *47*, 3955.
(9) Evans, O. R.; Lin, W. *Acc. Chem. Res.* **2002**, *35*, 511.
(10) Chen, B.; Wang, L.; Xiao, Y.; Fronczek, F. R.; Xue, M.; Cui, Y.; Qian, G. *Angew. Chem., Int. Ed.* **2009**, *48*, 500.
(11) Lan, A.; Li, K.; Wu, H.; Olson, D. H.; Emge, T. J.; Ki, W.; Hong, M.; Li, J. *Angew. Chem., Int. Ed.* **2009**, *48*, 2334.
(12) Allendorf, M. D.; Houk, R. J. T.; Andruszkiewicz, L.; Talin, A. A.; Pikarsky, J.; Choudhury, A.; Gall, K. A.; Hesketh, P. J. *J. Am. Chem. Soc.* **2008**, *130*, 14404.
(13) Lee, J.; Farha, O. K.; Roberts, J.; Scheidt, K. A.; Nguyen, S. T.; Hupp, J. T. *Chem. Soc. Rev.* **2009**, *38*, 1450.
(14) Ma, L.; Abney, C.; Lin, W. *Chem. Soc. Rev.* **2009**, *38*, 1248.
(15) Hu, A.; Ngo, H. L.; Lin, W. *J. Am. Chem. Soc.* **2003**, *125*, 11490.
(16) Wu, C.-D.; Hu, A.; Zhang, L.; Lin, W. *J. Am. Chem. Soc.* **2005**, *127*, 8940.
(17) deKrafft, K. E.; Xie, Z.; Cao, G.; Tran, S.; Ma, L.; Zhou, O. Z.; Lin, W. *Angew. Chem., Int. Ed.* **2009**, *48*, 9901.
(18) Horcajada, P.; Serre, C.; Vallet-Regí, M.; Sebban, M.; Taulelle, F.; Férey, G. *Angew. Chem., Int. Ed.* **2006**, *45*, 5974.
(19) Horcajada, P.; Serre, C.; Maurin, G.; Ramsahye, N. A.; Balas, F.; Vallet-Regí, M. A.; Sebban, M.; Taulelle, F.; Férey, G. R. *J. Am. Chem. Soc.* **2008**, *130*, 6774.
(20) Rieter, W. J.; Pott, K. M.; Taylor, K. M. L.; Lin, W. *J. Am. Chem. Soc.* **2008**, *130*, 11584.
(21) Xie, Z.; Ma, L.; deKrafft, K. E.; Jin, A.; Lin, W. *J. Am. Chem. Soc.* **2010**, *132*, 922.
(22) Ma, L.; Xie, Z.; Jin, A.; Lin, W. *Angew. Chem., Int. Ed.* **2009**, *48*, 9905.
(23) Rathore, R.; Burns, C. L.; Guzei, I. A. *J. Org. Chem.* **2004**, *69*, 1524.

Published on Web 09/22/2010

Scheme 2

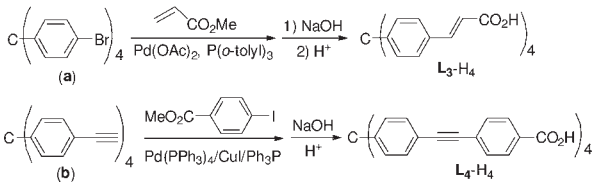

(Scheme 2). $\mathbf{L_4}$-H_4 was synthesized by a palladium-catalyzed Sonogashira coupling between tetrakis(4-ethynylphenyl)-methane (**b**)[25] and methyl 4-iodobenzoate followed by base-catalyzed hydrolysis. A solvothermal reaction between $\mathbf{L_3}$-H_4 and $Cu(NO_3)_2 \cdot 2.5H_2O$ in a dimethylformamide (DMF)/H_2O mixture under acidic conditions afforded blue crystals of $[Cu_2(\mathbf{L_3})(DMF)_2] \cdot 2DMF \cdot 4H_2O$ (**3**). A similar reaction between $\mathbf{L_4}$-H_4 and $Cu(NO_3)_2 \cdot 2.5H_2O$ in a diethylformamide (DEF)/H_2O mixture afforded blue crystals of $[Cu_2(\mathbf{L_4})(H_2O)_2] \cdot 12DEF \cdot 26H_2O$ (**4**; Scheme 1). These formulas were established based on single-crystal X-ray diffraction studies, ^{1}H NMR integration, and thermogravimetric analysis (TGA) results. TGA of **3** showed a solvent weight loss of 34.8% in the 20−200 °C temperature range (expected 33.4% for 2 DMF and 4 H_2O molecules), whereas TGA of **4** gave a significantly higher solvent weight loss of 63.1% in the 20−200 °C temperature range (expected 62.7% for 12 DEF and 26 H_2O molecules).

Single-crystal X-ray structure determination of **3** revealed an unprecedented three-dimensional (3D) homocrossing framework that crystallizes in the orthorhombic space group *Fddd*. In each asymmetric unit, there are three-quarters of ligand $\mathbf{L_3}$, one and a half of copper atoms, and one and a half of DMF molecules for the framework. The $\mathbf{L_3}$ ligand with the C1 central carbon atom (of $^1/_2$ occupancy) lying in the 2-fold axis ($^3/_8$, *y*, $^3/_8$) has a distorted tetrahedral geometry with a twist angle of 76.7° between the two planes formed by the C1 atom and copper paddle wheels. This twist angle is 90° for the $\mathbf{L_3}$ ligand, with the C2 central carbon atom (of $^1/_4$ occupancy) lying on a special position ($^5/_8$, $^5/_8$, $^5/_8$) with a site symmetry of 222. There exist two crystallographically distinct copper paddle wheels and tetrahedral ligands, as indicated with different colors in Figure 1a. Each unit cell includes 24 $\mathbf{L_3}$ ligands and 24 copper paddle-wheel SBUs, with 48 DMF molecules binding to the axial positions, leading to a framework formula of $[Cu_2(\mathbf{L_3})(DMF)_2]$. The tetrahedral ligands link the $[Cu(O_2CR)_4]$ SBUs to form a 3D, 4-connected, 4-nodal net of a new topology, with the Schläfli symbol $\{[4.6^2.8^3]^2[4^2.6^2.8^2][6^2.8^2.10^2][6^2.8^3.10]^2\}$.[26] This complicated connectivity can be described as network homocrossing. As shown in Figure 1a, two thick rings (green and pink) cross each other, which are interconnected by other parts of the network, shown as blue and orange linkages. Compound **3** has the largest open channels of 10 × 8.9 Å perpendicular to plane (−1, 9, 0) (Figure 1). *PLATON* calculations[27] of **3** indicated a void volume of 14 188 Å^3 (41.6% of the unit cell volume of 34 097 Å^3), which is consistent with the TGA result shown above.

(24) Ganesan, P.; Yang, X.; Loos, J.; Savenije, T. J.; Abellon, R. D.; Zuilhof, H.; Sudholter, E. J. R. *J. Am. Chem. Soc.* **2005**, *127*, 14530.
(25) Yuan, S.; Kirklin, S.; Dorney, B.; Liu, D.; Yu, L. *Macromolecules* **2009**, *42*, 1554.
(26) Blatov, V. A.; Shevchenko, A. P.; Serezhkin, V. N. *Russ. J. Coord. Chem.* **1999**, *25*, 453.
(27) Spek, A. L. *J. Appl. Crystallogr.* **2003**, *36*, 7.

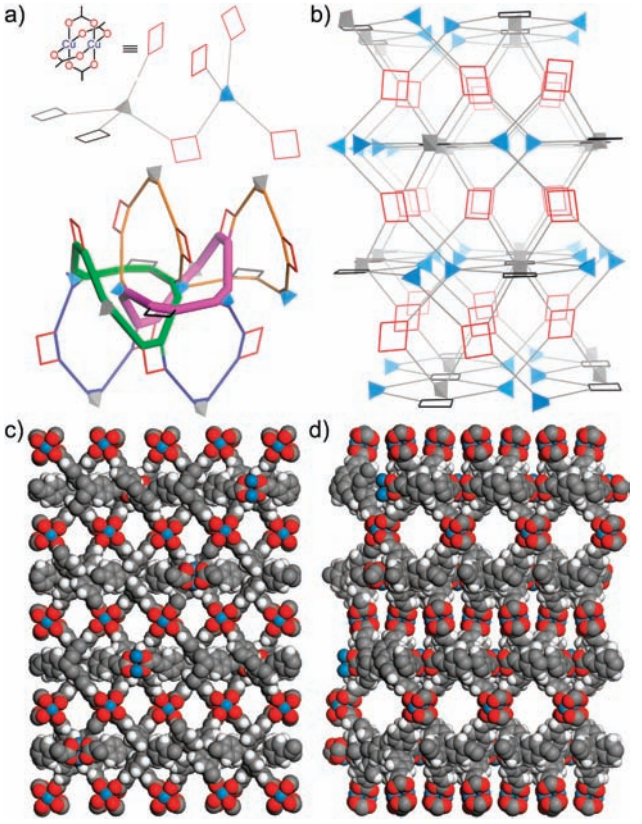

Figure 1. (a) Schematic representation of the tetracarboxylate ligand $\mathbf{L_3}$ (blue and gray tetrahedra) and copper paddle wheels (red and black squares) and their homocrossing pattern. (b) Schematic representation of the network connectivity of **3**. (c) Space-filling model **3** as viewed down the *a* axis. (d) Space-filling model of **3** as viewed perpendicular to the (−1, 9, 0) plane.

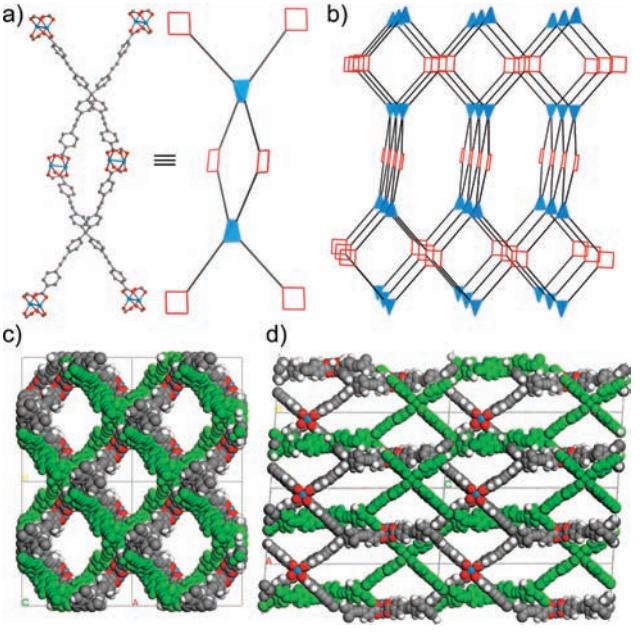

Figure 2. (a) Schematic representation of the tetracarboxylate ligand $\mathbf{L_4}$ (blue tetrahedra) and copper paddle wheels (red squares). (b) Schematic representation of the network connectivity of **3** of PtS topology. (c) Space-filling model of **3** as viewed down the *c* axis. (d) Space-filling model of **3** as viewed perpendicular to the (1, 1, 0) plane.

MOF **4** crystallizes in the monoclinic space group *C*2/*c* with a 2-fold interpenetrated PtS network topology. Each

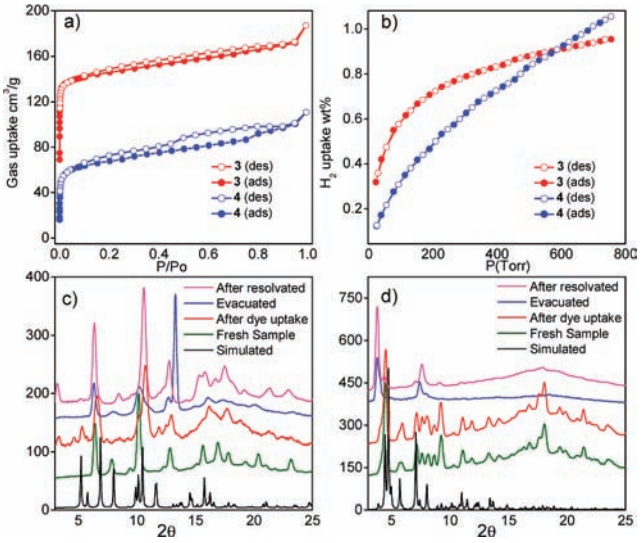

Figure 3. Nitrogen adsorption isotherms of MOFs **3** and **4** (a) at 77 K. Hydrogen adsorption isotherms of MOFs **3** and **4** (b) at 77 K. PXRD patterns of MOFs **3** (c) and **4** (d).

asymmetric unit contains one complete ligand $\mathbf{L_4}$, two copper atoms, and two coordinated water molecules (Figure 2). The space-filling model of **4** shows larger pore sizes than those of compound **3**, with the largest open channel of 25.6 × 10.6 Å perpendicular to the (1, 1, 0) direction. In agreement with TGA analysis, *PLATON* calculations of **4** indicated a void volume of 28 376 $Å^3$ (79.3% of the unit cell volume of 35 785 $Å^3$).

To further characterize the porosity of MOFs **3** and **4**, nitrogen and hydrogen adsorption experiments were performed at 77 K (Figure 3a,b). Both samples were pretreated by the freeze-drying method described in our previous work.[22] The freeze-dried sample of **3** exhibited a Langmuir surface area of 641 m^2/g (SA_{BET} of 555 m^2/g); however, the freeze-dried sample of **4** gave a Langmuir surface area of 272 m^2/g (SA_{BET} of 262 m^2/g). These relatively small surface area values may be attributed to the distortion and partial collapse of the frameworks after removal of the solvent molecules. On the basis of the powder X-ray diffraction (PXRD) patterns of **3** and **4** (Figure 3c,d), the distortion in framework **4** appears to be more severe, presumably as a result of larger channel sizes and thus reduced framework stability. The severe framework distortion of **4** also leads to the significant hysteresis in its nitrogen adsorption isotherms. Even with framework distortion, both **3** and **4** still show considerable hydrogen uptake capacity of 1.0 and 1.1 wt % at 1 atm of H_2 pressure, respectively.

A dye molecule inclusion study was also performed to verify the accessibility of the open channels of MOFs **1**−**4** in

(28) Ma, L.; Lin, W. *J. Am. Chem. Soc.* **2008**, *130*, 13834.

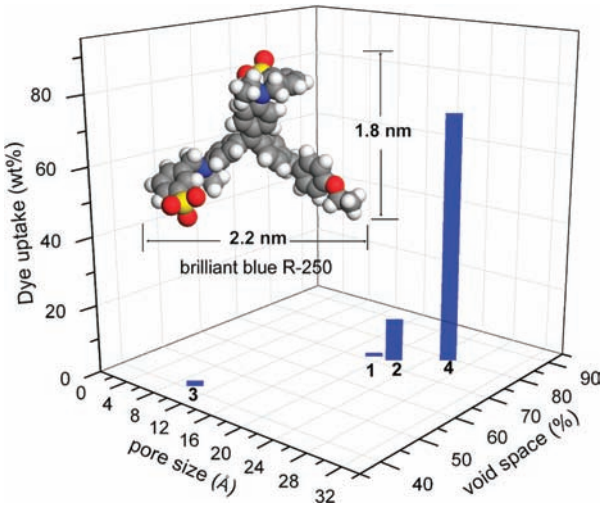

Figure 4. Uptake of BBR-250 dye by **1**−**4** illustrating the size selectivity. The inset shows the space filling of the energy-minimized structure of BBR-250 with dimensions.

solution.[28] Brilliant Blue R-250 (BBR-250), which has a molecular dimension of ~1.8 × 2.2 nm, was used in dye uptake experiments (Figure 4). MOF **4** has the highest dye uptake capacity (73 wt %) because of its largest channel size, compared with the other three MOFs (0.8 wt % for **1**, 12.4 wt % for **2**, and 1.4 wt % for **3**). The pore sizes of MOFs **1** and **3** are smaller than the dimensions of BBR-250, and therefore only a minimal amount of absorbed dye was detected, likely because of surface adsorption. The PXRD patterns of these dye-included MOFs are virtually the same as those of pristine MOFs (Figure 3c,d), indicating that the structural integrity and open channels of mesoporous MOFs are maintained in solution. There is a strong correlation between the dye uptake and channel size/void space in these MOFs. The dye uptake capacity thus provides an accurate determination of the permanent porosity of mesoporous MOFs.

In summary, we have synthesized new 4,4-connected MOFs with unprecedented homocrossing and interpenetrating PtS network topologies. These frameworks are highly porous, as indicated by their gas uptake and dye molecule inclusion capacity. Even with severe framework distortion, these MOFs show considerable hydrogen uptake capacity of 1.0 and 1.1 wt %, respectively.

Acknowledgment. We acknowledge financial support from the NSF and thank Athena Jin and Cheng Wang for experimental help.

Supporting Information Available: Experimental procedures, TGA results, ^{1}H NMR spectra, PXRD patterns, and an X-ray crystallographic file in CIF format. This material is available free of charge via the Internet at http://pubs.acs.org.